Amplified Spontaneous Emission and Lasing from Lanthanide-Doped Up-Conversion Nanocrystals

Hai Zhu,[†] Xian Chen,[‡] Li Min Jin,[†] Qi Jie Wang,[§,⊥] Feng Wang,[‡] and Siu Fung Yu[†,*]

[†]Department of Applied Physics, The Hong Kong Polytechnic University, Kowloon, Hong Kong SAR, China, [‡]Department of Physics and Materials Science, City University of Hong Kong, 83 Tat Chee Avenue, Kowloon, Hong Kong SAR, China, [§]School of Electrical and Electronic Engineering, Nanyang Technological University, Singapore 639798, and [⊥]School of Physical and Mathematical Sciences, Nanyang Technological University, Singapore 637371

ABSTRACT Lanthanide-doped nanocrystals (NCs), which found applications in bioimaging and labeling, have recently demonstrated significant improvement in up-conversion efficiency. Here, we report the first up-conversion multicolor microcavity lasers by using $NaYF_4$:Yb/Er@$NaYF_4$ core–shell NCs as the gain medium. It is shown that the optical gain of the NCs, which arises from the 2- and 3-photon up-conversion processes, can be maximized *via* sequential pulses pumping. Amplified spontaneous emission is observed from a Fabry–Perot cavity containing the NCs dispersed in cyclohexane solution. By coating a drop of silica resin containing the NCs onto an optical fiber, a microcavity with a bottle-like geometry is fabricated. It is demonstrated that the microcavity supports lasing emission through the formation of whispering gallery modes.

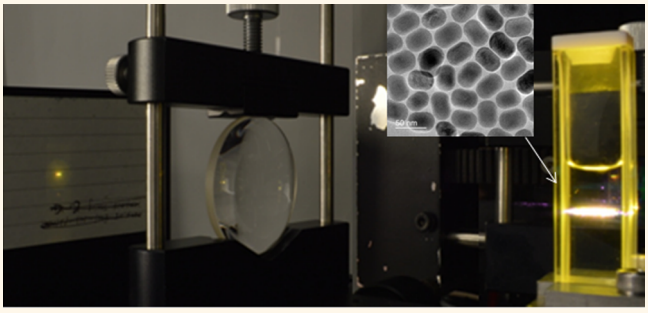

KEYWORDS: up-conversion nanoparticles · amplified spontaneous emission · microcavity lasers · whispering gallery modes

Up-conversion luminescence, which arises from the sequential absorption of two or more photons through intermediate energy states with long decay lifetime, has emission wavelength shorter than that of the excitation source.[1−3] Up-conversion materials can be fabricated by doping lanthanide ions into hosts of low phonon-energy.[4] Recently, novel design and synthesis of surface passivated lanthanide-doped nanocrystals (NCs) have been demonstrated with significant improvement in up-conversion efficiency.[5,6] This is because of the reduction of surface quenching effects and the suppression of energy transfer from the dopant ions to the crystal surface. On the other hand, biomolecules and biomolecular assemblies such as live cells can also be integrated with surface passivated NCs due to its surface wetting characteristics.[7] Hence, extensive concentration has been investigated on the use of lanthanide-doped NCs as the 'perfect' luminescent probes for the biological imaging and labeling applications.[2,8]

However, how effective is the luminescence obtained from lanthanide-doped NCs *via* up-conversion process when compared to that from the conventional optical materials? As stimulated emission required large quantity of population inversion, efficiency of up-conversion process can be verified through the realization of lasing. Hence, the demonstration of lasing emission is an unambiguous verification on the potential usage of up-conversion process in photonics and biological applications. However, to the best of our knowledge, neither amplified spontaneous emission nor stimulated emission has been observed from the lanthanide-doped NCs.[9,10] This may due to the following two reasons: (1) lack of appropriate pumping scheme to achieve simultaneously sufficient population inversion and low optical damage of the NCs, and (2) difficulty in assembling up-conversion NCs of nanoscale geometry as optical gain media. In this communication, optical characteristics of the up-conversion $NaYF_4$:Yb/Er@$NaYF_4$ core–shell NCs under a 980 nm wavelength excitation were studied at room temperature. A 3-pulse pumping scheme was developed to maximize the output intensity of the

* Address correspondence to sfyu21@hotmail.com.

Received for review October 16, 2013 and accepted November 23, 2013.

Published online November 24, 2013
10.1021/nn405387t

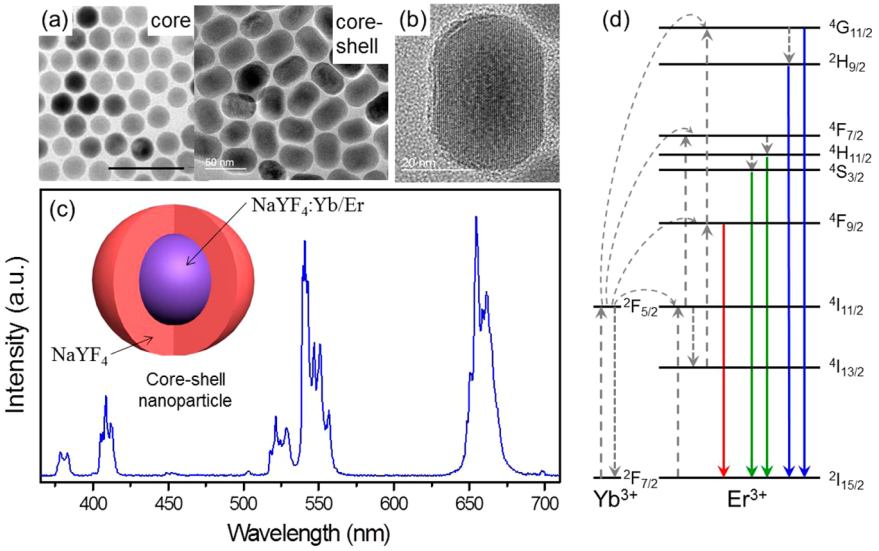

Figure 1. (a) Typical TEM images of the as-synthesized $NaYF_4$:Yb/Er core and $NaYF_4$:Yb/Er@$NaYF_4$ core−shell NCs. (b) HR-TEM image of the NCs as shown in (a). (c) Room-temperature up-conversion photoluminescent spectra of the NCs dispersed in cyclohexane solution under CW 980 laser excitation. (d) Proposed energy transfer mechanism of the $NaYF_4$:Yb/Er@$NaYF_4$ core−shell NCs.

core−shell NCs under pulses excitation while without damaging the NCs. Hence, optical gain of the up-conversion NCs at wavelengths around 410, 540, and 655 nm was studied. By dispersing the NCs in cyclohexane solution, amplified spontaneous emission was observed from a Fabry−Perot (FP) cavity containing the NCs solution. Furthermore, a bottle-like microcavity was fabricated by coating a mixture of silica resin and NCs onto an optical fiber. It is demonstrated that the microcavity supports lasing emission through the formation of whispering gallery modes. Hence, we verified unambiguously that the up-conversion NCs are a promising optical media to realize high-performance up-conversion optical devices.

RESULTS AND DISCUSSION

Figure 1 reveals the physical and optical characteristics of the $NaYF_4$:Yb/Er@$NaYF_4$ core−shell NCs to be used for the realization of lasers. Transmission electron microscopy (TEM) images of the core and core−shell NCs are shown in Figure 1a. The elongated core−shell NCs mainly result from the anisotropic shell growth during the coating process, which is commonly observed from hexagonal phase $NaYF_4$ nanocrystals.[11,12] The average length and diameter of the core−shell NCs are ~45 and ~35 nm, respectively, and these have a standard derivation of ~3 nm. Figure 1b shows the high-resolution TEM images of the core−shell NCs. It is observed that the lattice spacing between the (100) plane of the core−shell NCs is ~0.515 nm. Figure 1c plots the emission spectrum of the core−shell NCs under the excitation of a continuous-wave (CW) 980 nm laser. Five dominant emission peaks at around 655, 540, 525, 410, and 380 nm emerge from the emission spectrum. The rise of these emission peaks can be explained by the energy transfer mechanism plotted in Figure 1d. Emission peaks at 655, 540, and 525 nm are attributed to 2-photon up-conversion process, while those at wavelength of 410 and 380 nm are due to 3-photon up-conversion process. Decay lifetime of all these fluorescence peaks was also measured and listed (see Supporting Information, Table S1). Due to the different in decay lifetime, it is expected that 410 and 540 nm peaks will dominate over the peaks at 380 and 525 nm, respectively, if the core−shell NCs are used to support lasing emission.

There are challenges to be overcome in order to realize up-conversion lasing emission from the rare-earth doping NCs. First, what kind of excitation method (*e.g.*, CW or pulses excitation) can achieve high optical gain and avoid optical damage? Second, what will be the most appropriate laser cavity? For the first question, neither the use of high CW pumping (*i.e.*, problem of optical damage) nor the application of single pulse excitation (*i.e.*, insufficient population inversion due to simultaneously 2- and 3-photon up-conversion processes) can achieve enough optical gain. To overcome this problem, a 3-pulse excitation system was constructed (Figure 2). This system generates three 980 nm pulses with pulsewidth and time delay between adjacent pulses equal to 6 and 10 ns, respectively, at a repetition rate of 10 Hz. Hence, the advantages of high peak power and relatively short in the duration of high power irradiation (*i.e.*, low optical damage) can be obtained simultaneously for achieving larger population inversion. It must be noted that the pulsewidth and delay time should be shorter than that of the carrier decay lifetime of the NCs. Figure 3 verifies the use of sequential pulses pumping on the improvement of the up-conversion efficiency of the

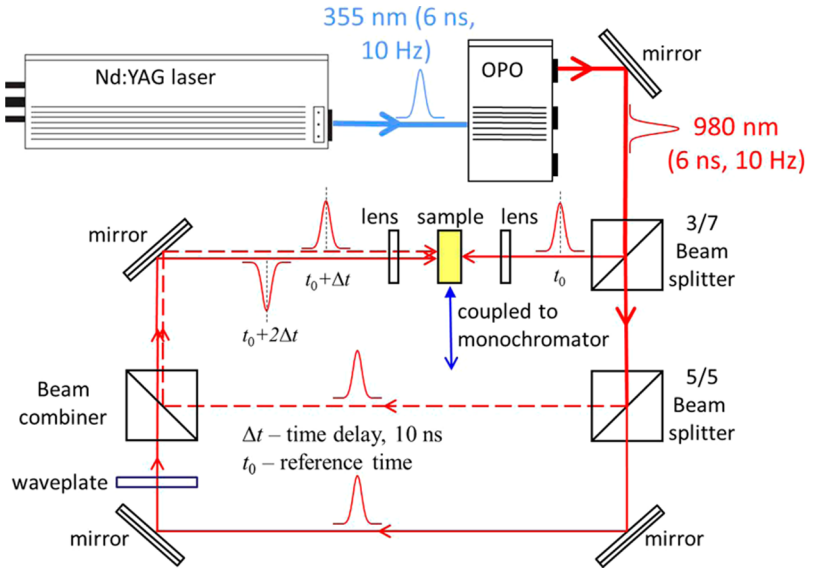

Figure 2. Experimental setup of a 980 nm 3-pulse excitation system. Three continuous pulses with pulsewidth and time delay of 6 and 10 ns respectively are generated from a Nd:YAG laser *via* an optical parametric oscillator. The repetition rate of the pulses is equal to 10 Hz. The laser system generated 2 laser beams. First laser beam consists of single pulse and the second beam combines 2 pulses with a time delay of 10 and 20 ns with respect to the first laser beam. The 2 laser beams are focused by cylindrical lenses to 2 pump stripes of width ~30 μm. In order to achieve effective pumping, the 2 pump stripes are 'spatially' overlapped.

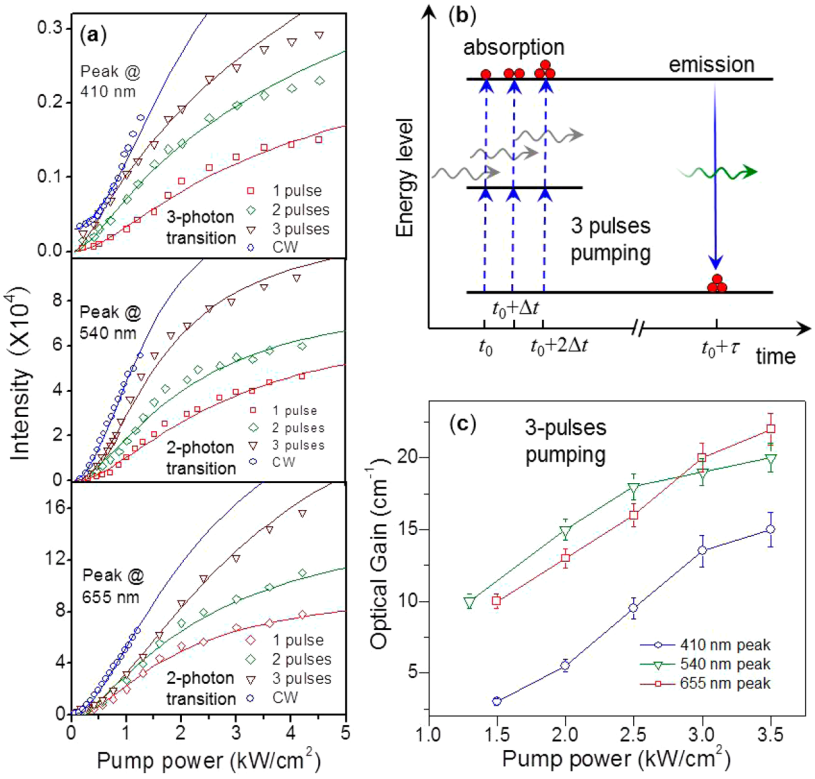

Figure 3. (a) Up-conversion emission characteristics of the $NaYF_4$:Yb/Er@$NaYF_4$ core–shell NCs under different excitation schemes (*i.e.*, 1-pulse, 2-pulse, 3-pulse and CW excitation). The pulsewidth and delay time remain unchanged for different excitation schemes (except CW excitation). (b) Schematic diagram showing the population dynamic alignment under 3-pulse laser excitation with 10 ns delay. (c) Optical gain of the three color bands (*i.e.*, 410, 540, and 655 nm) *versus* different pump power of the 3-pulse excitation scheme.

NCs. In the experiment, $NaYF_4$:Yb/Er@$NaYF_4$ core–shell NCs dispersed in cyclohexane with concentration of 3.6 wt % were placed in a quartz cuvette. The as-synthesized NCs are surface capped with oleate ligands and can be well dispersed in nonpolar solvents such as cyclohexane. We chose cyclohexane as solvent

mainly due to its large optical transparence, low toxicity, and easy extraction of the nanocrystals from the solvent. The low boiling point of cyclohexane also facilitates its removal through evaporation. The sequential three pulses were focused onto the quartz cuvette along the same horizon by two cylindrical lenses with a focal length of 5 cm. Similarly, single and double pulses (with the same pulsewidth and time delay) were also used to excite the NCs. Figure 3a shows that the output intensity of the NCs under 3-pulse excitation is higher than that of the single and 2-pulse excitation and approaches that of CW pumping. This implies that 3-pulse excitation can improve the up-conversion efficiency of NCs under pulses excitation.

Emission mechanism of 2- and 3-photon up-conversion processes can be elucidated by a simple rate equation analysis (see Supporting Information).[13] The output intensity for 2-photon, $I_{2p}(t)$, and 3-photon, $I_{3p}(t)$, up-conversion processes *versus* input excitation power, $\langle W\rangle$, can be written as

$$I_{2p}(t) = \frac{C_0\langle W\rangle^2}{C_1 + C_2\langle W\rangle + C_3\langle W\rangle^2}\{1 - \exp[-(C_1 + C_2\langle W\rangle + C_3\langle W\rangle^2)t]\} \quad (1)$$

$$I_{3p}(t) = \frac{D_0\langle W\rangle^3}{D_1 + D_2\langle W\rangle + D_3\langle W\rangle^2 + D_4\langle W\rangle^3}\{1 - \exp[-(D_1 + D_2\langle W\rangle + D_3\langle W\rangle^2 + D_4\langle W\rangle^3)t]\} \quad (2)$$

where t is the excitation duration and $\langle W\rangle$ is the spatial average power density of the excitation pulses. The constants C_0, C_1, C_2, C_3, D_0, D_1, D_2, D_3 and D_4 can be deduced from the measured data and the corresponding values are given in Table S2. The solid lines in Figure 3a represent the fitting of eqs 1 and 2 for the cases of 2-photon and 3-photon up-conversion processes, respectively, under either 1-pulse, 2-pulse, 3-pulse or CW excitation. Figure 3b explains the reason why the output intensity *via* 3-pulse excitation can approach the conversion efficiency of CW excitation. As the total delay time of the pulses is shorter than the decay lifetime of carriers at the upper energy state, the amount of population inversion can be increased by using 3-pulse excitation.

Conversion efficiency of $NaYF_4$:Yb/Er@$NaYF_4$ core–shell NCs can also be investigated by measuring the corresponding net optical gain, $G(\lambda)$, which is also a function of wavelength, λ, *via* the variable stripe length (VSL) method.[14] Figure 3c plots G (with λ equal to 410, 540, and 655 nm) *versus* pump power (under 3-pulse excitation at 980 nm) of the NCs. For low power excitation, optical gain at wavelength of 540 nm is the highest. However, the corresponding optical gain saturates with the increase of excitation power (*i.e.*, >2.5 kW/cm^2). This may be due to the saturation of population inversion at the $^4F_{7/2}$ level under high excitation power so that the corresponding carrier decay lifetime is reduced. Optical gain of blue and red bands, however, remains roughly proportional to the excitation power.

For the second question, we constructed a FP cavity with $NaYF_4$:Yb/Er@$NaYF_4$ core–shell NCs dispersed in cyclohexane with concentration of 3.6 wt % as the gain medium (Figure 4a). The FP cavity consists of a quartz tube sandwiched between a distributed Bragg reflector (DBR) and an Al mirror. Figure 4b plots the reflectivity of the two DBRs and an Al mirror to be used in the experiment. It is noted that the peak reflectivity of the DBR 1 and DBR 2 is about 95% at wavelength (with bandwidth) of ~410 (~50) and ~550 nm (~200 nm), respectively. The Al film has a reflectivity of 95% over a range of wavelength between 410 and 655 nm. Hence, DBR 1 and DBR 2 were used to study the emission characteristics of the FP cavity between the blue and red color bands. In the experiment, the FP cavity was excited by 2 pump stripes of width less than 30 μm along the length (on the same horizon) of quartz tube *via* focusing of 2 laser beams obtained from the 3-pulse excitation system. The emission intensity was detected from the DBR. Figure 4c shows the normalized emission spectra of the FP cavity at room temperature. As expected, emission peaks emerge at wavelength around 410, 540, and 655 nm due to their relatively long decay lifetime in their color bands. Furthermore, these emission peaks collapsed into narrow sharp peaks with the increase of excitation power. Panels d and e of Figure 4 plot the nonlinear spectrally integrated output power and line width, respectively, *versus* excitation power of these peaks. It is observed that the narrowing of emission peaks starts to occur for the pump power reaches a threshold value, P_{th} (*i.e.*, the kinks in Figure 4d). It is noted that the green (blue) band has the lowest (highest) P_{th} due to its relatively high (low) optical gain (see also Figure 3c). The output intensity of the green emission band increases linearly above P_{th} even at high excitation power (>2.5 kW/cm^2). No saturation of output intensity indicates that the population inversion at $^4F_{7/2}$ level is clamped at P_{th} but the saturation of output does not occur. Furthermore, the emission line width can be reduced by more than four times of its initial value. Hence, these clearly shown that the $NaYF_4$:Yb/Er@$NaYF_4$ core–shell NCs support amplified spontaneous emission in FP cavity. Nevertheless, due to the long cavity length, fine structures of the lasing spectra are not observed.

To reveal lasing emission, optical fiber microcavities with a bottle-like geometry were fabricated.[15] This can be done by mixing the $NaYF_4$:Yb/Er@$NaYF_4$ core–shell NCs with silica resin and coated onto optical fibers with different diameter. The concentration of NCs in silica resin is maintained at 3.6 wt %. Figure 5a plots the emission spectra of the microcavity with diameter equal to 80 μm *versus* pump power. The microcavity was excited by 2 pump stripes (with width <30 μm) in

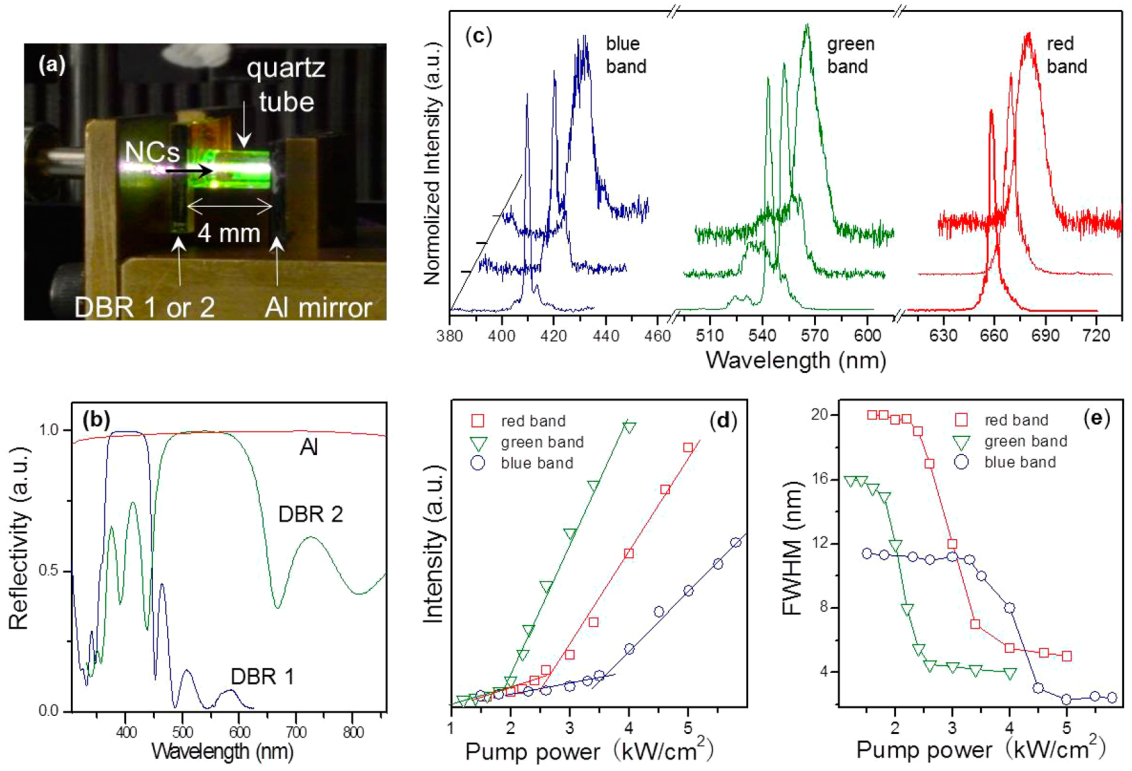

Figure 4. (a) Image of the FP cavity using $NaYF_4$:Yb/Er@$NaYF_4$ core−shell NCs dispersed in cyclohexane solution as the gain medium. (b) Reflection spectra of DBRs and Al mirror. (c) Plot of normalized photoluminescent spectra of the 3 color bands *versus* different excitation power based on the 3-pulse excitation scheme. (d) Light−light curves and (e) FWHM of three color band as a function of the different excitation power.

the direction perpendicular to the fiber (on the same horizon position). The pump stripes were realized by focusing 2 laser beams obtained from the 3-pulse excitation system. At low excitation power (*i.e.*, <5.0 kW/cm^2), three broad spontaneous emission bands (*i.e.*, center peaks at around 408, 540, and 654 nm) emerge from the emission spectrum. For excitation power above 5.5, 6.5, and 8.5 kW/cm^2, well-defined narrow sharp peaks are excited from the emission bands with center wavelength at around 407, 540, and 655 nm, respectively. The full-width at half-maximum of the narrow sharp peaks is less than 0.2 nm. The measured mode spacing, $\Delta\lambda$, is found to be around 0.43, 0.72, and 1.03 nm for the center wavelength equal to 407, 540, and 655 nm, respectively. These findings are consistent with $\Delta\lambda$ of spherical microcavities:[16]

$$\Delta\lambda = \lambda_0^2/\pi D n_{\text{eff}} \quad (3)$$

where λ_0 (=407, 540, or 655 nm) is the center peak wavelength, n_{eff} (=1.6) is the effective refractive index and D is the diameter of microcavities. The inset of Figure 5a gives the near-field images of the microcavity (D = 80 μm) under different excitation power. It is observed that the lasing light is mainly emitted along the radial direction of the microcavity.

Figure 5b plots the output intensity *versus* pump power (in double log scale) of the three emission bands. The emission output exhibits a well-known S-like behavior with three distinguished regions of different slopes. At low excitation power (*i.e.*, below P_A), the region represents the regime of spontaneous emission. For the region between P_A and P_{th}, the output intensities increase superlinearly with slope much larger than that at the low excitation region. Further increase of excitation power above P_{th} indicates the above threshold operation of the microcavity. These three regions represent the transition from spontaneous emission (*i.e.*, < P_A) through amplified spontaneous emission (*i.e.*, between P_A and P_{th}) to laser oscillation.

Figure 5c shows the measured and fitted values of the threshold P_{th} *versus* D for the three lasing bands (with center peak wavelength equal to 407, 540, and 655 nm). It is observed that the values of P_{th} increases with the decrease of diameter D. For the optical fiber microcavities with a bottle-like geometry, we can write[17]

$$P_{th} \propto \exp(-\alpha D) \quad (4)$$

where α is curvature loss. The solid lines represent the fitting of measured data with eq 4. It can show that the curvature loss ratio of the three emission bands $\alpha_{blue}/\alpha_{green}/\alpha_{red}$ is about 3:5:6. This is reasonable because lasing modes with shorter wavelength have lower radiation loss than those that have longer wavelength of the same microcavity. The inset of Figure 5c plots the measured values of mode spacing $\Delta\lambda$ *versus* 1/D for the

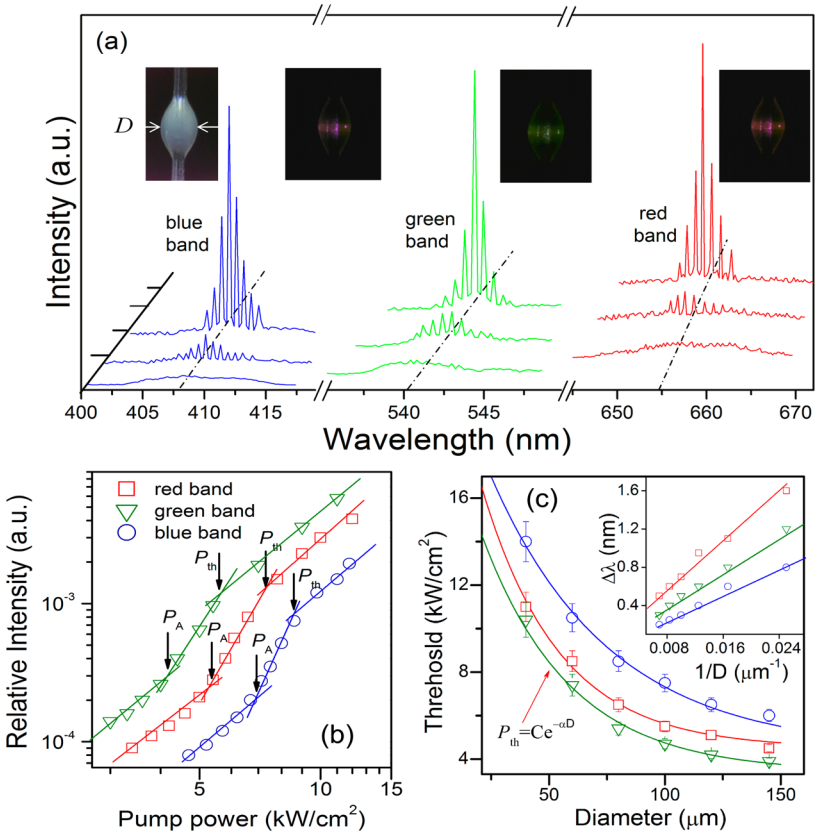

Figure 5. (a) Lasing spectra of the microcavity with a bottle-like geometry of diameter equal to 80 μm under 3-pulse excitation scheme at room temperature. The insets show the images of the microcavity under different excitation power. (b) Log−log plot of output power *versus* pump power for the three color bands of the microcavity. (c) Measured and fitted (solid lines) values of P_{th} and $\Delta\lambda$ (inset figure) *versus* D for the three color bands of the microcavity.

three emission bands. By using eq 3 to fit the measured data for the three lasing bands, it is deduced that the value of n_{eff} is ~1.58 which is in consistent with the estimate value of n_{eff}. Hence, it is verified that the resonance of whispering gallery modes supported by the microcavities demonstrated the lasing characteristics.

CONCLUSIONS

In conclusion, amplified spontaneous emission and lasing were demonstrated from $NaYbF_4$:Yb/Er@$NaYF_4$ core−shell NCs *via* 2- and 3-photon up-conversion processes. By using a sequential pulse pumping, emission intensity of the NCs can be maximized. Hence, amplified spontaneous emission was realized from a FP cavity containing the NCs dispersed in cyclohexane solution under pulse excitation. Narrowing of emission peaks from the three color bands was observed simultaneously. In addition, no saturation of output intensities implies that the population inversion is clamped at P_{th} and amplify stimulate emission at green band does not occur at high excitation power. Furthermore, a microcavity with bottle-like geometry was fabricated by coating silica resin dispersed with the NCs onto an optical fiber. Lasing emission of the three color bands was demonstrated simultaneously under pulse excitation. It was found that the lasing mechanism of the microcavity is due to the excitation of WGMs. Hence, we have verified unambiguously that the $NaYF_4$:Yb/Er@$NaYF_4$ core−shell NCs exhibited high up-conversion efficiency and can be used as the gain medium to achieve lasing emission under 980 nm pulse excitation.

METHODS

$NaYF_4$:Yb/Er@$NaYF_4$ Core−Shell NCs. The $NaYF_4$:Yb/Er@$NaYF_4$ core−shell NCs were synthesized by coprecipitation and the corresponding fabrication procedures can be found from our previous report.[18]

TEM. By using a JEM-2010 TEM, the morphology of the $NaYbF_4$:Yb/Er@$NaYF_4$ core−shell NCs was studied. This can be done by dispersing the NCs onto the Cu/lacey-carbon TEM grids. Scanning TEM images, which were obtained by using a field-emission TEM operated at 200 kV, were measured at a 2-μs/pixel scanning rate. High-resolution bright-field TEM imaging was carried out using a high-resolution TEM operated at 200 kV.

Sequential Pulses Pumping (3-Pulse Excitation). The laser system consists of a Continuum Panther EX optical parametric oscillator under the excitation by a 355 nm frequency-tripled Continuum Powerlite DLS 9010 Q-switched Nd: YAG laser. Wavelength, pulsewidth, and repetition rate of the optical pulses obtained from this laser system were equal to 980 nm, 6 ns, and 10 Hz,

respectively. The laser beam was split into three portions with roughly equal intensity by passing through a 30/70 (reflection %/transmission %) beam splitter and then to a 50/50 beam splitter. One of the beams (*i.e.*, the first pulse) was focused onto the right-hand-side of the sample *via* a cylindrical lens to a pump stripe of width ~30 μm. The remained two beams, after traveling for either a distance L (*i.e.*, second pulse) or 2L (third pulse), were combined together through a polarization dependent beam splitter and a quarter waveplate. The combined beam was focused onto the left-hand-side of the sample *via* another cylindrical lens to a pump stripe of width ~30 μm. In the experiment, the three beams must ensure to be spatially overlapped on the same location of the sample. In addition, L is selected such that the delay time of the second and third pulses is equal to 10 and 20 ns, respectively.

FP Cavity. The FP laser cavity consists of a quartz tube of 4 mm long with inner and outer diameters of 1 and 2 mm, respectively. The quartz tube was filled with NCs dispersed in cyclohexane has concentration of 3.6 wt %. The two ends of the quartz tube were terminated by a DBR and an Al coated mirror and sealed by silica resin. The 3-pulse excitation system was used to excite the NCs inside the quartz tube. The emission light was collected from the DBR through an optical fiber of 400 μm aperture. An Oriel MS257 monochromator attached with a photomultiplier tube was used to analyze the emission spectrum of the FP cavity. To study the blue (green and red) emission band, DBR 1 (DBR 2) was used to construct the FP cavity.

Bottle-like Geometry Optical Fiber Microcavities. A bare optical fiber was coated with a small drop of mixture of NCs and silica resin. The coated optical fiber was then hung in a vertical orientation and under optical excitation by the 3-pulse excitation system. It must be noted that the pump stripes should be oriented perpendicular to the length of the optical fiber on the top surface of the bottle resonator. The emission light was then collected from the surface of the microcavity through an optical fiber of 400 μm aperture.

VSL Method. The $NaYF_4$:Yb/Er@$NaYF_4$ core−shell NCs dispersed in cyclohexane was placed in a quartz cuvette (stand vertically) and was pumped by the 3-pulse excitation method. It is noted that two horizontal pump stripes of width <30 μm were focused on the left- and right-hand side (longer side) of the quartz cuvette. Emission obtained from the shorter side of the quartz cuvette was then collected through an optical fiber of 400 μm aperture. If the length of the pump stripes, L_S, and the emission intensity obtained from the shorter side of the quartz cuvette, I_{tot}, were measured, then the corresponding optical gain, $G(\lambda)$, for some pump power could be deduced through the classical VSL equation:

$$I_{tot}(L,\lambda) = I_{sp}(\lambda)(\exp[G(\lambda)L_S] - 1)/G(\lambda) \quad (5)$$

where I_{sp} is the spontaneous emission intensity.

Conflict of Interest: The authors declare no competing financial interest.

Acknowledgment. This work was supported by HK PolyU grants (Grant Nos. G-YX4P and G-YJ73).

Supporting Information Available: Details of materials for the decay lifetime of the up-conversion emission peaks at different wavelength, rate equation analysis, the experimental setup to measure the emission characteristics of NCs dispersed in cyclohexane solution under 980 nm laser excitation, and the simulation of WGMs in the bottle-like microcavity. This material is available free of charge *via* the Internet at http://pubs.acs.org.

REFERENCES AND NOTES

1. Haase, M.; Schäfer, H. Upconverting Nanoparticles. *Angew. Chem., Int. Ed.* **2011**, *50*, 5808.
2. Cheng, L.; Wang, C.; Liu, Z. Upconversion Nanoparticles and Their Composite Nanostructures for Biomedical Imaging and Cancer Therapy. *Nanoscale* **2013**, *5*, 23–37.
3. Wang, F.; Liu, X. G. Recent Advances in the Chemistry of Lanthanide-doped Upconversion Nanocrystals. *Chem. Soc. Rev.* **2009**, *38*, 976–989.
4. Pollnau, M.; Gamelin, D. R.; Luthi, S. R.; Gudel, H. U.; Hehlen, M. P. Power Dependence of Upconversion Luminescence in Lanthanide and Transition-Metal-Ion Systems. *Phys. Rev. B.* **2000**, *61*, 3337–3346.
5. Wang, F.; Wang, J.; Liu, X. G. Direct Evidence of a Surface Quenching Effect on Size-Dependent Luminescence of Upconversion Nanoparticles. *Angew. Chem., Int. Ed.* **2011**, *49*, 7456–7460.
6. Yi, G.; Chow, G. Water-Soluble $NaYF_4$:Yb, Er(Tm)/$NaYF_4$/Polymer Core/Shell/Shell Nanoparticles with Significant Enhancement of Upconversion Fluorescence. *Chem. Mater.* **2007**, *19*, 341.
7. Wang, M.; Abbineni, G.; Clevenger, A.; Mao, C.; Xu, S. Upconversion Nanoparticles: Synthesis, Surface Modification and Biological Applications. *Nanomedicine* **2011**, *12*, 710–729.
8. Chatteriee, D. K.; Rufalhah, A. J.; Zhang, Y. Upconversion Fluorescence Imaging of Cells and Small Animals Using Lanthanide doped Nanocrystals. *Biomaterials* **2008**, *29*, 937–943.
9. Dong, C. H.; Yang, Y.; Shen, Y. L.; Zou, C. L.; Sun, F. W.; Ming, H.; Guo, G. C.; Han, Z. F. Observation of Microlaser with Er-Doped Phosphate Glass Coated Microsphere Pumped by 780 nm. *Opt. Commun.* **2010**, *283*, 5117–5120.
10. Wu, Y. Q.; Ward, J. M.; Chormaic, S. N. Ultralow Threshold Green Lasing and Optical Bistability in ZBNA (ZrF4−BaF2−NaF−AlF3) Microspheres. *J. Appl. Phys.* **2010**, *107*, 033103.
11. Zhang, C.; Lee, J. Y. Prevalence of Anisotropic Shell Growth in Rare Earth Core-Shell Upconversion Nanocrystals. *ACS Nano* **2013**, *7*, 4393–4402.
12. Wen, H.; Zhu, H.; Chen, X.; Hung, T. F.; Wang, B.; Zhu, G.; Yu, S. F.; Wang, F. Upconverting Near-Infrared Light through Energy Management in Core−Shell−Shell Nanoparticles. *Angew. Chem., Int. Ed.* DOI: 10.1002/anie.201306811.
13. Yahel, E.; Hardy, A. Modeling High-power Er^{3+}-Yb^{3+} Codoped Fiber Lasers. *J. Lightwave Technol.* **2003**, *21*, 2044–2052.
14. Velenta, J.; Pelent, I.; Linnros, J. Waveguiding Effects in the Measurement of Optical Gain in a Layer of Si Nanocrystal. *Appl. Phys. Lett.* **2002**, *81*, 1396–1398.
15. Kavokin, A.; Baumberg, J. J.; Malpuech, G.; Laussy, F. P. *Microcavities*; Oxford University Press: Oxford, 2007.
16. Pöllinger, M.; O'Shea, D.; Warken, F.; Rauschenbeutel, A. Ultrahigh-Q Tunable Whispering-Gallery-Mode Microresonator. *Phys. Rev. Lett.* **2009**, *103*, 053901.
17. Faustini, L.; Martini, G. Bend Loss in Single-Mode Fibers. *J. Lightwave Technol.* **1997**, *15*, 671–679.
18. Wang, F.; Deng, R. R.; Wang, J.; Wang, Q. X.; Han, Y.; Zhu, H. M.; Chen, X. Y.; Liu, X. G. Tuning Upconversion through Energy Migratin in Core-Shell Nanoparticles. *Nat. Mater.* **2011**, *10*, 968–973.